ADVANCED OPTICAL MATERIALS
www.advopticalmat.de

Metasurface-Enhanced Photon Upconversion upon 1550 nm Excitation

Doğuşcan Ahiboz, Elina Andresen, Phillip Manley, Ute Resch-Genger, Christian Würth, and Christiane Becker**

Photon upconversion upon 1550 nm excitation is of high relevance for applications in the third biological excitation window, for photovoltaics beyond current limitations, and enables appealing options in the field of glass fiber telecommunications. Trivalent doped erbium ions (Er^{3+}) are the material of choice for 1550 nm excited upconversion, however, they suffer from a low absorption cross-section and a low brightness. Therefore, the ability of silicon metasurfaces to provide greatly enhanced electrical near-fields is employed to enable efficient photon upconversion even at low external illumination conditions. Hexagonally shaped β-$NaYF_4$:Er^{3+} nanoparticles are placed on large-area silicon metasurfaces designed to convert near-infrared (1550 nm) to visible light. More than 2400-fold enhanced photon upconversion luminescence is achieved by using this metasurface instead of a planar substrate. With the aid of optical simulations based on the finite-element method, this result is attributed to the coupling of the excitation source with metasurface resonances at appropriate incident angles. Analysis of the excitation power density dependence of upconversion luminescence and red-to-green-emission ratios enables the estimation of nanoscale near-field enhancement on the metasurface. The findings permit the significant reduction of required external excitation intensities for photon upconversion of 1550 nm light, opening perspectives in biophotonics, telecommunication, and photovoltaics.

1. Introduction

Photon upconversion (UC) is a process in which at least two photons of low energy are absorbed and a single photon with higher energy is emitted. The ability to convert light from the near-infrared (NIR) to the visible spectral region opens new possibilities to overcome current limitations in solar energy,[1,2] and to enable autofluorescence-free biosensing and -imaging,[3–5] temperature sensing (nanothermometry),[6] and nanoscale electric field sensing.[7] Trivalent erbium (Er^{3+})-doped crystals are widely used for photon UC as they exhibit ladder-like separated energy levels[8] lying within the near-infrared biological excitation windows and which are accessible with commercially available excitation sources.

However, lanthanide ions such as Er^{3+} have a comparably small absorption cross-section[9] which results in a poor brightness and hence small signals under near-infrared excitation.[10] Particularly for excitation in the first biological window (700–950 nm),[11] the Er^{3+} absorption cross-section is so small such that they are often integrated in a host crystal which is codoped with another rare earth ion with a larger absorption cross-section such as trivalent ytterbium as sensitizer. By contrast, for excitation around 1550 nm – a wavelength regime that is of particular interest in the application areas of telecommunication, biology, and photovoltaics – Er^{3+} is the material of choice which can be directly excited, avoiding the necessity of a codoping material.

In every case, photon UC is a nonlinear optical process and its efficiency critically depends on excitation power density (P_{exc}). A nowadays widely discussed approach to increase the UC efficiency is to harvest the strongly enhanced near fields in the vicinity of dielectric or plasmonic nanostructures. For photon UC with lanthanide-doped materials, several studies have been published demonstrating more than two orders of magnitude enhanced photon UC upon excitation around 980 nm using plasmonic[12] or dielectric[7,13–16] structures. Particularly, Liang et al. set a benchmark by the demonstration of five orders of magnitude enhanced UC using a dielectric superlensing array on large areas up to 50 cm^2.[16] Regarding UC upon excitation in the 1500 nm regime, there exist few pioneering studies reporting on enhanced photon UC by

D. Ahiboz, P. Manley,[+] C. Becker
Department Optics for Solar Energy
Helmholtz-Zentrum Berlin für Materialien und Energie
Albert-Einstein-Str. 16, 12489 Berlin, Germany
E-mail: christiane.becker@helmholtz-berlin.de

E. Andresen, U. Resch-Genger, C. Würth
Division Biophotonics
Federal Institute for Materials Research and Testing (BAM)
Richard-Willstaetter-Str. 11, 12489 Berlin, Germany
E-mail: christian.wuerth@bam.de

P. Manley
Computational Nano Optics Group
Zuse Institute Berlin
Takustr. 7, 14195 Berlin, Germany

The ORCID identification number(s) for the author(s) of this article can be found under https://doi.org/10.1002/adom.202101285.

[+]Present address: JCMwave GmbH, Bolivarallee 22, 14050 Berlin, Germany

DOI: 10.1002/adom.202101285

(nano)concentration of light.[17–20] However, these works suffer from limited enhancement values[17,19,20] or employ small-scale plasmonic nanostructures,[18] severely restricting its practicability in photovoltaics and the bioassay technology. On the other hand, dielectric metasurfaces have recently attracted great attention due to their opportunity for low dissipative losses, large resonant enhancement of electromagnetic near fields,[21] and applicability on larger area.[22]

Here, we show enhanced UC luminescence emission of $NaYF_4:Er^{3+}$ nanoparticles (NPs) deposited onto a large-area (25 cm^2) dielectric silicon metasurface fabricated by soft-nanoimprint lithography and thin-film deposition techniques. We demonstrate more than three orders of magnitude enhanced UC luminescence emission upon 1550 nm laser excitation at distinct incident angles. Optical simulations allow to attribute the UC luminescence enhancement by the coupling of metasurface resonances with the 1550 nm laser excitation beam. Furthermore, UC dynamics on the silicon metasurface are investigated by means of excitation-power-dependent luminescence emission and ratios of the red-to-green emission intensities, allowing to estimate the strength of nanoscale electromagnetic near fields.

2. Results and Discussion

Oleate-capped $NaYF_4:Er^{3+}$ NPs were synthesized using thermal decomposition by choosing reaction conditions that favor the formation of larger particles.[23] As revealed by the transmission electron microscopy (TEM) images in **Figure 1**, the synthesized NPs are nanoplates with an average size of 130 nm × 60 nm. The elemental composition of the NPs was determined by inductively coupled plasma optical emission spectrometry (ICP-OES) showing Y^{3+} and Er^{3+} contents provided in percentage of the total amount of lanthanides of (74.2 ± 1.3) mol% and (25.8 ± 1.5) mol%, respectively. This Er^{3+} doping level was chosen as a starting point for several reasons: concentrations in this range have been proposed for solar cell applications.[2,24] It has also been demonstrated that the strength of cross-relaxations is acceptable within this concentration range[25,26] and that the absorption cross-section of the particles is not limiting to the experiments. There is of course a trade-off between these two effects. The radiative electronic transitions of the β-$NaYF_4:Er^{3+}$ nanocrystals corresponding to distinct UC emission peaks are indicated by comparison with the literature in Figure 1b.[26,27] The luminescence emission of the β-$NaYF_4:Er^{3+}$ NPs, from 350 to 1020 nm, in cyclohexane solution is shown in Figure 1c. The spectral data were collected for a continuous wave laser excitation with a power density of P_{exc} = 52 W cm^{-2} and λ_{exc} = 1551 nm. A photograph of the luminescence emission in a 1 mm thick cuvette that has been placed inside an integrating sphere is shown in the inset of Figure 1c.

The geometrical design of the photon UC system is illustrated in **Figure 2**a. In order to quantify the metasurface-induced UC luminescence enhancement, the emission intensities of $NaYF_4:Er^{3+}$ NPs on metasurface and on a planar part of the silicon film are compared. The excitation beam is tilted along one of the metasurface high-symmetry directions Γ–K or Γ–M (see inset). The silicon metasurface is designed as a hexagonal nanohole array with lattice constant p = 1000 nm, hole diameter d = 400 nm, and layer thickness of t = 53 nm. A scanning electron microscopy (SEM) image of the produced silicon metasurface is shown in Figure 2b. The β-$NaYF_4:Er^{3+}$ NPs are deposited on the metasurface via drop-casting to form a layer with an average thickness of 660 nm. A top view SEM image of the β-$NaYF_4:Er^{3+}$ NPs on the metasurface is shown in Figure 2c. A cross-section SEM image of the β-$NaYF_4:Er^{3+}$ NPs on the silicon metasurface is depicted in Figure 2d. More details regarding the silicon metasurface production on nanoimprinted glass can be found in Figures S1 and S2 (Supporting Information) and in ref. [28].

Angularly resolved luminescence measurements (see Figure S3 in the Supporting Information) were performed under laser excitation with both, transverse-electric (TE)- and transverse-magnetic (TM)-polarized light, with λ_{exc} = 1551 nm at P_{exc} = 30 W cm^{-2}. The angular dependence of the UC luminescence emission in **Figure 3**a is obtained by sweeping the angle of incidence (AoI) from 0° to 40° along the Γ → M high symmetry direction of the metasurface. For each measurement point, the whole emission spectrum (as shown in Figure 1c) is integrated from 350 to 1020 nm. The integrated emission exhibits three distinct peaks at AoI = 8° ± 1° and 18° ± 1° under the TE-polarized excitation (orange shaded horizontal lines) and AoI = 26° ± 1° for TM-polarized excitation (blue shaded horizontal lines) in Figure 3a.

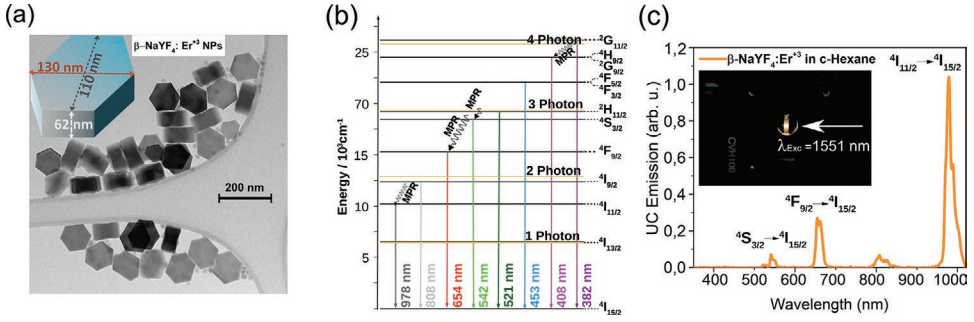

Figure 1. Properties of the hexagonal β-$NaYF_4:Er^{3+}$ nanoparticles (NPs) in solution. a) TEM image of the β-$NaYF_4:Er^{3+}$ upconversion (UC) NPs with the inset illustrating the dimensions. b) Energy level diagram of the UC NPs with radiative transitions between the electronic levels of the Er^{3+} indicated. c) Typical UC luminescence emission spectrum of the UC NPs in cyclohexane solution. The inset shows a photographic image of the NP/cyclohexane solution in 1 mm thick cuvette placed inside an integrating sphere upon 1550 nm laser excitation.

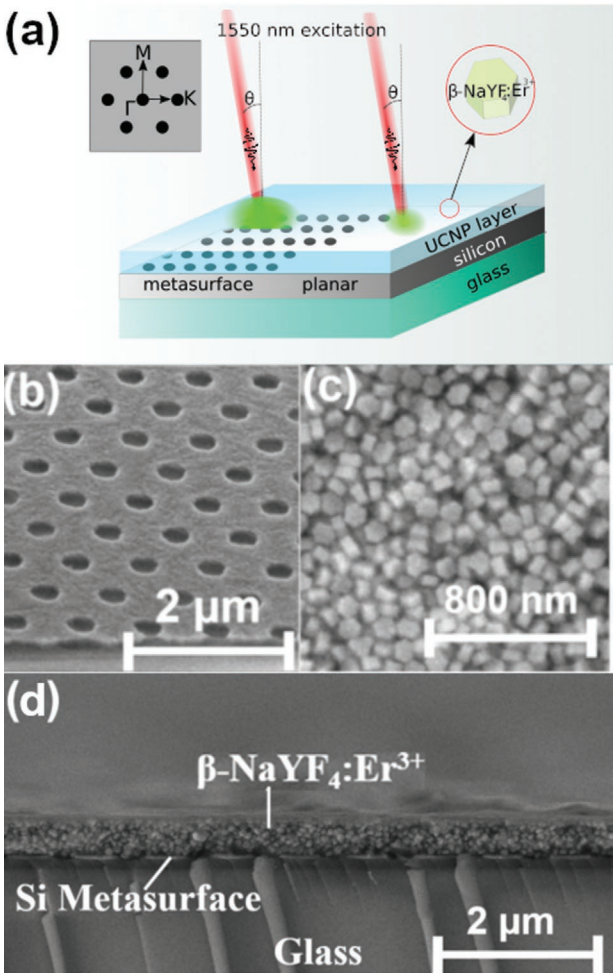

Figure 2. Photon UC system designed to convert near-infrared (1550 nm) to visible light. a) Schematic of the UC system comprised of a silicon metasurface covered with a β-$NaYF_4$:Er^{3+} NP layer as well as geometrical details of the experimental setup designed for UC enhancement investigation. b) Scanning electron microscopy (SEM) image of the uncovered silicon metasurface, taken at viewing angle 30°. c) Top view on the β-$NaYF_4$:Er^{3+} NP layer on metasurface. d) SEM cross-section image of a 660 nm thick β-$NaYF_4$:Er^{3+} NP layer covering the silicon metasurface, respectively. The planar appearance on top of the NP layer can be regarded as an artefact due to charging effects during the SEM measurements.

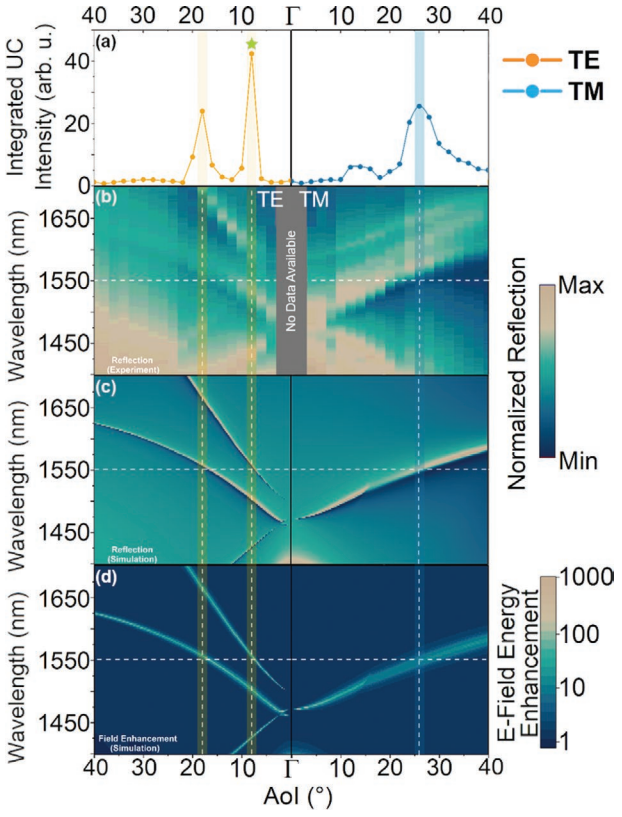

Figure 3. Correlation between enhanced upconversion emission and excitation of metasurface resonances. a) Integrated UC emission (350–1020 nm) from β-$NaYF_4$:Er^{3+} NPs on silicon metasurface as function of the angle of incidence (AoI) for rotation in $\Gamma \rightarrow M$ high symmetry direction using TE (left)- and TM (right)-polarized 1551 nm radiation for excitation (P_{exc} = 30 W cm^{-2}). b) Experimentally measured and c) simulated reflectance of the β-$NaYF_4$:Er^{3+} NP/silicon metasurface system. The color bar ranges from 15% to 50% for a better visibility in case of (b) and from 0 to 1 in case of (c). d) Calculated enhancement of the electrical near-field energy inside the β-$NaYF_4$:Er^{3+} NP layer volume (compared to the respective electric field energy in the same volume in free space). White dashed lines represent laser excitation wavelength at 1551 nm, while orange and blue shaded white lines represent the angle of incidences where the luminescence emission maxima are observed.

To elucidate the origin of the enhanced UC emission at distinct AoIs, we studied the so-called leaky modes of the silicon metasurface. Leaky modes of metasurfaces are resonances, which can couple with external radiation and can be excited by choosing an appropriate combination of angle of incidence AoI and excitation wavelength λ_{exc}. These modes are often associated with strongly enhanced near fields on the metasurface[29] and can increase the number of absorbed photons in the β-$NaYF_4$:Er^{3+} NP layer considerably. Coupling with leaky modes often shows up as resonant features in optical transmittance or reflectance measurements.[30] Here, the angularly resolved reflectance measurement (ARRM) method is employed (see Figure S3 in the Supporting Information). The ARRMs of the β-$NaYF_4$:Er^{3+}-NP-coated silicon metasurface reveal the spectral dispersion of the leaky modes, which are the dark and light resonant patterns in Figure 3b, spanning the NIR region from 1400 to 1700 nm under rotation along the $\Gamma \rightarrow M$ high symmetry direction for TE (left)- and TM (right)-polarized light. The presence of the resonant features at 1551 nm excitation can be traced by the orange and blue shaded vertical lines. It can be clearly seen that the peaks of the integrated UC emission of β-$NaYF_4$:Er^{3+} correspond to the same AoIs where resonant features occur in the ARRM for λ_{exc} = 1551 nm. An ARRM on a bare silicon metasurface without UC NP layer is shown in Figure S4 (Supporting Information). Here, the resonant features are slightly shifted toward shorter wavelengths due to the lack of the UC NP layer.

To obtain a better understanding of the origin of the luminescence enhancement of β-$NaYF_4$:Er^{3+} NPs on the metasurface and expand the understanding of our experimental results, ARRM spectra of β-$NaYF_4$:Er^{3+} NPs on a silicon metasurface were also simulated using the finite-element method. The

presence of the two leaky TE modes and one TM leaky mode interacting with 1551 nm excitation is shown in Figure 3c. An excellent agreement of the spectral position of resonances in reflectance in experiment (Figure 3b) and simulation (Figure 3c) can be observed. Furthermore, angularly and spectrally resolved near fields on the silicon metasurface were calculated (Figure 3d). The electric field energy enhancement is defined by the total electrical field energy integrated over the volume of the β-$NaYF_4$:Er^{3+} layer on the silicon metasurface, divided by the respective electric field energy in the same volume in free space. Electric field energy enhancement values of up to 1000 are obtained by simulation, which are similar to values presented in the literature,[7,29,31] and are in agreement with the spectral and angular positions of the leaky modes of the silicon metasurface. For TM-polarized light at AoI around 15°, a weak additional feature is observed for both measured integrated UC and ARRM. We attribute this small discrepancy between experiment and simulations to a weak contribution of the $\Gamma \rightarrow$ K high symmetry direction caused by a slight disorientation of the metasurface imprinting process. Considering the overall agreement of angular positions exhibiting enhanced UC emission (Figure 3a), resonant features in the experimental (Figure 3b) and simulated (Figure 3c) reflectance, and simulated enhanced near fields (Figure 3d) strongly indicate that the increase of the UC luminescence of β-$NaYF_4$:Er^{3+} NPs on silicon metasurface is attributed to the excitation of leaky metasurface modes associated with strong near fields.

A detailed analysis of the simulated electric field distribution of the specific resonance associated with the strongest UC emission for excitation with TE-polarized light and AoI = 7.3° is illustrated in **Figure 4**. It shows the spatial distribution of the electric field energy w_e normalized to the electric field energy in the same volume for the incident wave in vacuum w_e^0 (detailed equations to calculate w_e^0 and w_e can be found in the Supporting Information). The cross-sectional x–z- and y–z-planes shown in Figure 4b,c indicate that these enhanced near fields leak out of the silicon metasurface by about 200–300 nm. Hence, no more than half of the UC NP layer volume experiences enhanced electric fields. The distribution in the x–y-plane (Figure 4a) shows a pattern with close to the sixfold symmetry of the lattice. From all the three resonances that can be excited with 1551 nm light, this specific resonance exhibits the smallest full width at half maximum (see Figure S5 in the Supporting Information) and hence a higher quality factor and a higher buildup of localized energy. The electric field energy density plots of the other two resonances occurring at 1551 excitation (TE with AoI = 16.7°; TM with AoI = 27.2°) can be found in Figure S6 (Supporting Information).

Further examination of the near-field effects on the UC process was investigated by P_{exc}-dependent measurements. β-$NaYF_4$:Er^{3+}-NP-coated silicon metasurface and planar silicon reference were excited at AoI = 8°, where a leaky mode of silicon metasurface exists at 1550 nm. The P_{exc} dependence of the UC emission is expressed by a so-called power law[32]

$$\log I \propto n \cdot \log P_{exc} + \text{const} \tag{1}$$

where I is the UC emission intensity. The value of n is equal to the slope of a linear fit to the data of I versus P_{exc} on a double-logarithmic scale. In the limit of low P_{exc} and low concentration of Er^{3+} (i.e., less than 1%), the value for n approaches the number of photons involved in the excitation process. The P_{exc} dependence of UC emission in double-logarithmical representation based on the $^4I_{11/2} \rightarrow {}^4I_{15/2}$ transition (978 nm) and $^4F_{9/2} \rightarrow {}^4I_{15/2}$ transition (654 nm) is shown in Figure S7 (Supporting Information). **Figure 5**a,b depicts the slope factors n extracted from these power-dependent data by differentiating Equation (1). It is expected that energy transfer is an important upconversion mechanism for materials doped with 26% Er^{3+}[33] as utilized in this study. The excitation power dependence of the energy transfer upconversion (ETU) under low excitation intensities can be described by Equation (1). The slope factors of the 978 nm ($^4I_{11/2} \rightarrow {}^4I_{15/2}$) and 654 nm ($^4F_{9/2} \rightarrow {}^4I_{15/2}$) transitions approach values of around 2 and 3 at low excitation intensities, respectively, indicating two and three photons involved for UC. As we do not see significant blue and ultraviolet emission, we regard the impact of populated high energy levels and the corresponding cross-relaxation processes that are known to populate the red (654 nm) transition ($^4F_{9/2} \rightarrow {}^4I_{15/2}$)[33] as negligible for both, using a silicon metasurface and a planar silicon reference, in the range of our experimental conditions. With increasing P_{exc}, however, the slope factors quickly decrease to 0.5 and 1 in case of 978 and 654 nm emissions, respectively, which is in accordance with the work by Pollnau et al. from 2000:[32] the slope factors for ETU when the transition includes the ground state result in n = 0.5 for 978 nm emission and n = 1 for the next higher level, with increasing excitation intensity.

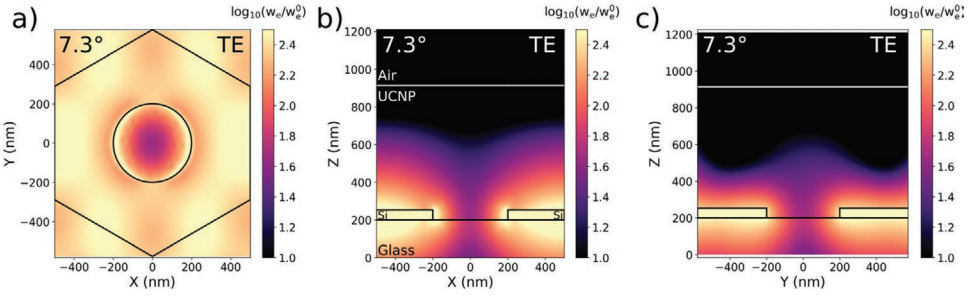

Figure 4. The logarithm of the electric field energy density in cross-sectional planes of the simulated hexagonal unit cell of the metasurface for TE-polarized light incident with an angle of 7.3° at 1551 nm. a) The x–y-plane is evaluated at z = 1 nm above the silicon surface. The b) x–z- and c) y–z-planes are evaluated at y = 0 and x = 0, respectively. In part (b), the materials of the sample – UC NP, silicon (Si), and glass – are indicated. w_e and w_e^0 designate the electric field energies in a given region and in the same volume for the incident wave in vacuum, respectively.

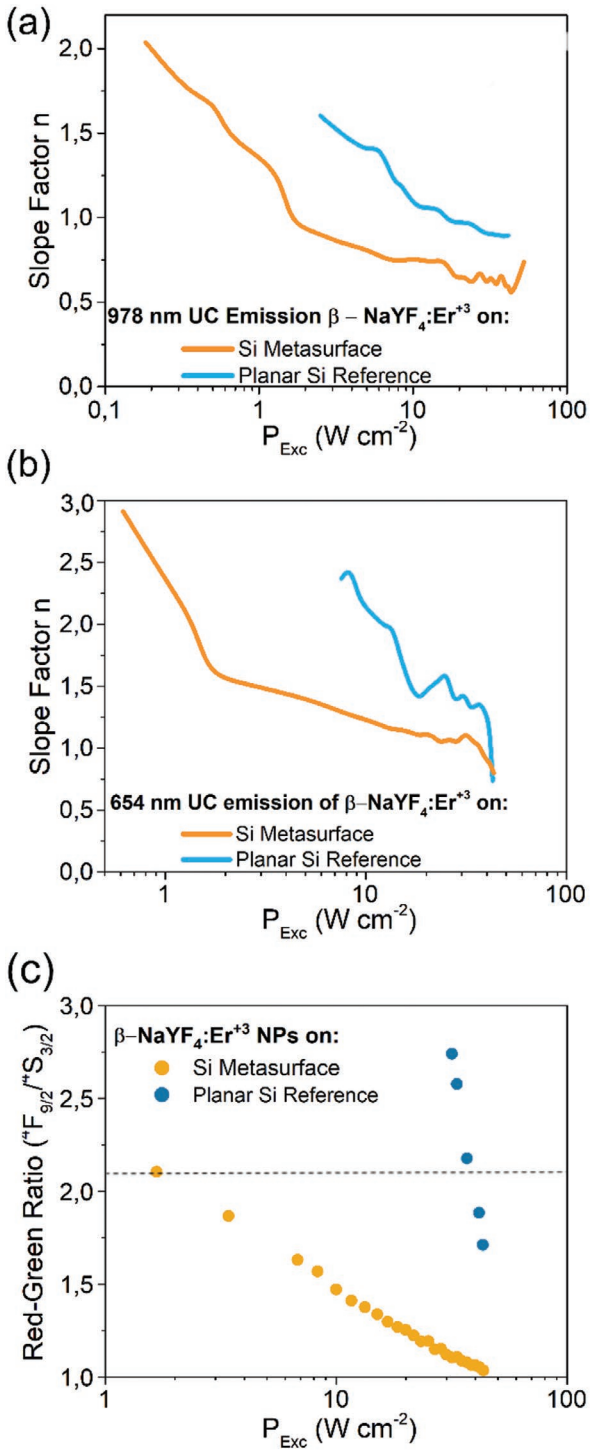

Figure 5. Power dependence of upconversion luminescence from β-$NaYF_4$:Er^{3+} nanoparticles on silicon metasurfaces (orange symbols/lines) and planar silicon films (blue symbols/lines). a,b) Slope factors n (5-point-average) from Equation (1) extracted from UC emission intensity versus 1550 nm excitation power density P_{exc} in double-logarithmical representation, for the UC emission peaks at 987 and 654 nm, respectively (see Figure S5 in the Supporting Information). c) Red-to-green (654/542 nm) UC emission ratio as function of P_{exc}. All measurements were taken at AoI = 8° with TE-polarized light at λ_{exc} = 1550 nm, hence on metasurface resonance excitation conditions.

Interestingly, the dependency of the slope factor n of the 978 nm emission on P_{exc} (Figure 5a) for both the silicon metasurface and planar silicon reference has a similar shape, occurring at different values of P_{exc}. Hence, starting with a silicon metasurface substrate, P_{exc} needs be increased by over an order of magnitude to obtain similar slope factors using a planar Si substrate. A similar trend is observed for the red transition ($^4F_{9/2} \rightarrow {}^4I_{15/2}$) in Figure 5b. The slope of the 654 nm emission reaches n = 3 for low excitation power densities, as expected for a three photon UC process. At higher power densities, slope values n = 1.5–1.8 are observed for the red emission of the Er^{3+}-doped crystals, which is in agreement with reports from the literature at 1.5 µm laser excitation.[34,35] Also here, similar n values on the metasurface can be obtained at more than one order of magnitude lower excitation power densities P_{exc} than on planar silicon films. These are further indications of enhanced near fields on the metasurface.

The P_{exc} dependence of the red-to-green (654/542 nm) emission ratios is compared both on the silicon metasurface and planar silicon reference at AoI = 8° in Figure 5c. Both, $^4F_{9\backslash2}$ and $^4S_{3\backslash2}$ levels of the Er^{3+}, are excited by at least three photons (Figure 1b). In the following text, we assume that equal near-field intensities within the UC NP layer would lead to equal red-to-green ratios in the UC spectra. That means an external excitation power density of only around 1.9 W cm^{-2} in case of the metasurface yields a comparable red-to-green-ratio like 43 W cm^{-2} in the case of the planar silicon layer (dashed line). The metasurface enables similar red-to-green emission ratios with around 23-fold reduced P_{exc}. In a first rough approximation, considering a slope factor n of around 1.7 for the red transition at P_{exc} = 1.9 W cm^{-2} (see Figure 5b), an UC emission enhancement of $23^{1.7}$–200 is estimated. However, the extraction of an absolute value of the near-field enhancement on the metasurface is challenging: the enhancement factor of a luminescent process on a metasurface also depends on how well the upconverter material and the near fields spatially overlap, i.e., it depends on the distance of the UC material from the metasurface. As already shown in Figure 4, in our sample system with around 660 nm thick UC NP layer and only 53 nm thin silicon metasurface, we expect maximum half of the UC NPs being exposed to enhanced near fields of the resonantly excited metasurface.

The effect of the near-field enhancement is further studied by comparing UC emission intensity of the β-$NaYF_4$:Er^{3+} NPs on silicon metasurface and on planar silicon reference as function of the excitation beam AoI for rotation in $\Gamma \rightarrow$ M direction of the metasurface, TM-polarized light, P_{exc} = 52 W cm^{-2}, and λ_{exc} = 1550 nm (**Figure 6**a). The explicitly measured UC emission on the silicon metasurface and on the planar reference at 978, 654, and 542 nm are shown in Figure S8 (Supporting Information). At the two resonant angles (AoI = 8° and AoI = 18°) that had already been identified by ARRM (Figure 3), enhanced UC emission ratios up to 100, 300, and 800 times for the 978, 654, and 542 nm emission peaks are achieved. These enhancement factors lie in the same range as estimated from comparing red-to-green-emission ratios above. Similar results on luminescent enhancement values using dielectric and metallic metasurfaces were already demonstrated by others.[31] The difference in enhancement factors can be attributed to considerably different

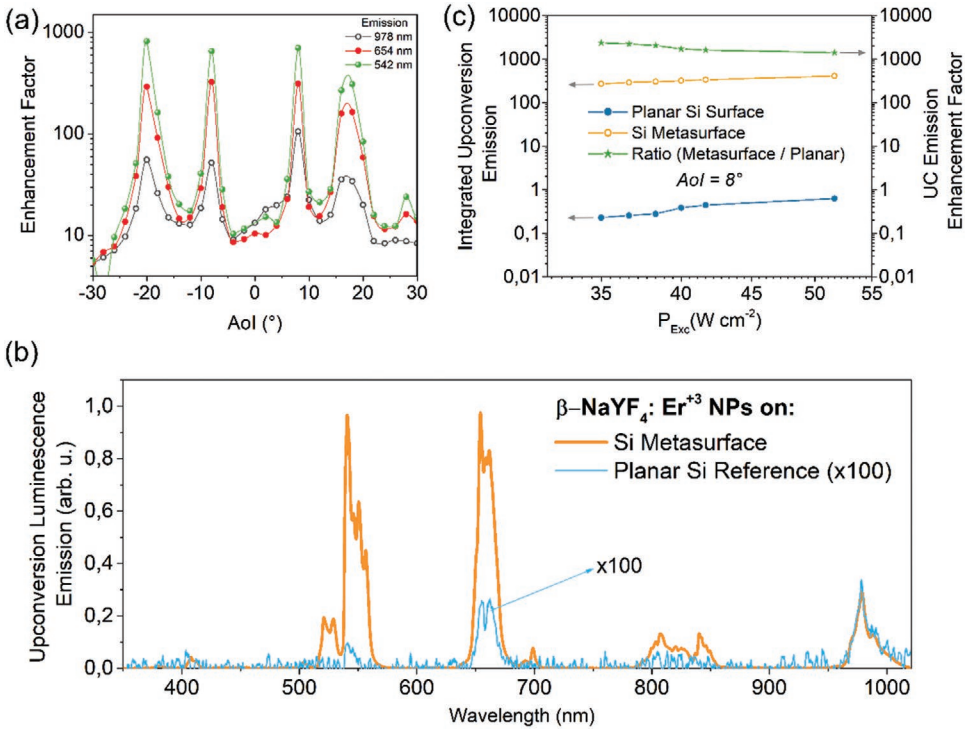

Figure 6. Evaluation of metasurface-enhanced UC emission. a) Ratio of the UC emission of β-$NaYF_4$:Er^{3+} NPs on silicon metasurface and planar silicon reference films for the emission peaks at 978, 654, and 542 nm (as indicated) as function of the excitation beam angle of incidence AoI (rotation in $\Gamma \rightarrow M$ direction of the metasurface, $P_{exc} = 52$ W cm^{-2}, and $\lambda_{exc} = 1550$ nm). b) Upconversion luminescence emission spectra at 8° angle of incidence of the silicon metasurface (orange curve and planar silicon reference (blue curve, magnified by a factor of 100). c) Integrated UC emission intensity of β-$NaYF_4$:Er^{3+} NPs on silicon metasurface (orange hollow dots) and on planar silicon reference (blue solid dots), and upconversion enhancement factor as function of excitation power density P_{exc}.

population dynamics for the three investigated emission wavelengths. As a result from the power law $I \propto P_{exc}^n$, the emission intensities I depend with different powers n on the excitation power density P_{exc} for the three different emission wavelengths, resulting in larger enhancement factors for large n values and smaller enhancement factors for smaller n values. This explains the smaller enhancement factor of the UC emission at 978 nm (a 2-photon absorption process) compared to the observed enhancement factors at 542 nm (3 or more photons involved). The 654 nm band lies in between 987 and 545 nm and can be populated via several other pathways. The decreasing red-to-green emission ratio with increasing excitation power density shown in Figure 5c is an experimental evidence that the n factor of the red emission is smaller than the respective n of the green emission, explaining smaller metasurface-induced enhancement factors. Moreover, enhanced upconversion emission by around one order of magnitude is observed at every AoI even without contribution of a metasurface leaky mode. The observed emission enhancement effect at nonresonant AoIs might be attributed to both, better extractions of the upconverted photons from the nanostructured metasurface and light trapping in the β-$NaYF_4$:Er^{3+} NP layer that might be caused by total internal reflection of higher diffraction orders on the metasurface.[20]

Figure 6b shows two UC emission spectra of NPs on metasurface (orange lines) and planar silicon (blue lines, 100 times magnified) for 8° AoI excitation. Hence, when exciting a metasurface resonance (which is indicated by a green star in Figure 3a) for an excitation power density of $P_{exc} = 52$ W cm^{-2}, a vast difference in emission intensity is observed which reflects the effect of the enhanced near fields on the absorption of β-$NaYF_4$:Er^{3+} NPs. Furthermore, the shape of the emission spectrum changes considerably, e.g., by means of a different red-to-green emission ratio (compare Figure 5c). The integrated UC luminescence of the β-$NaYF_4$:Er^{3+} NPs was also measured for a wider range of P_{exc} values between 35 and 52 W cm^{-2} by integrating the UC emission bands from 500 to 1021 nm (Figure 6c). Remarkable metasurface-induced UC enhancement factors from 1150 ($P_{exc} = 52$ W cm^{-2}) to even 2430 ($P_{exc} = 35$ W cm^{-2}) are observed (green symbols and lines). The metasurface-induced enhancement of the integrated UC emission intensity increases with decreasing excitation power density P_{exc}, and there is reason to believe that even higher enhancement factors can be expected at lower P_{exc} values. As already seen in Figure 5, the integrated UC emissions from β-$NaYF_4$:Er^{3+} NPs exhibit different power dependence on the silicon metasurface and planar silicon reference. This provides a hint that the near fields on the silicon metasurface can change the population dynamics and the UC mechanism considerably.

3. Conclusion

We demonstrated more than 2400-fold enhanced upconversion emission of β-$NaYF_4$:Er^{3+} nanoparticles by placing them on a

silicon metasurface. This enhancement is ascribed to strong near fields originating from the coupling between metasurface resonances with the 1550 nm laser excitation at resonant incident angles. A detailed study of the excitation-power-density-dependent upconversion dynamics providing slope factors and red-to-green-emission-ratios of the upconverted emission yields an indirect tool to quantify nanoscale-enhanced near fields. The obtained results open up possibilities to dramatically reduce the required external excitation power densities for optical applications based on photon upconversion upon excitation in the third biological excitation window (1550–1870 nm). In light of the fact that in our sample system only a part of the 660 nm thick upconversion nanoparticle layer experiences enhanced near fields from the metasurface, even stronger effects can be expected by attaching the upconversion nanoparticles in a monolayer on the metasurface, which is practical for many applications, e.g., biosensing. This could greatly increase the spatial overlap between leaky mode volume and upconversion particles and give rise to even higher enhancements factors. These findings are expected not only to allow for dramatically reduced detection limits in biosensing but also to help harnessing near-infrared parts of the solar spectrum, which cannot be used by state-of-the-art silicon photovoltaic devices. Moreover, this provides an elegant tool to quantify nanoscale electromagnetic near fields on nanostructures by exclusively applying far-field spectroscopic measuring technologies around 1550 nm, the conventional band for telecommunications.

4. Experimental Section

Synthesis of $NaYF_4$:Er^{3+} Nanoparticles: Oleate-capped $NaYF_4$:Er^{3+} was synthesized following a procedure reported by Wilhelm et al. for the large-scale synthesis of hexagonal-phase UC NPs with some modifications.[23] Briefly, $YCl_3{\cdot}6H_2O$ (1213.4 mg, 4.0 mmol) and $ErCl_3{\cdot}6H_2O$ (381.7 mg, 1.0 mmol) were dissolved in 15 mL of methanol by sonication and subsequently added to a mixture of oleic acid (30 mL) and 1-octadecene (75 mL) in a 250 mL three-necked flask. The stirred reaction mixture was then heated to 150 °C under argon flow. After 30 min, vacuum was applied for further 45 min at 150 °C to remove remaining low-boiling impurities. The lanthanide precursor-containing reaction mixture was then cooled down to room temperature under a constant argon flow. Subsequently, a methanolic solution (30 mL) containing NaOH (500 mg, 12.5 mmol) and NH_4F (740 mg, 20 mmol) was added, and the resulting suspension was heated to 120 °C for 30 min to remove excess methanol. The reaction mixture was heated to 325 °C under reflux while applying a gentle flow of argon and kept at this temperature for 90 min. Then, the reaction mixture was cooled down to room temperature and the nanoparticles were precipitated by ethanol and collected by centrifugation at 5000 rpm for 5 min. Then, the NPs were redispersed in chloroform, washed by ethanol several times, and stored in cyclohexane (c = 30 mg mL^{-1}) at 4 °C.

Characterization of $NaYF_4$:Er^{3+} Nanoparticles: The dopant ratio was verified by ICP-OES (Spectro Arcos, Spectro Analytical Instruments GmbH, Kleve, Germany).

TEM images were obtained with a Talos F200S Microscope (Thermo Fisher Scientific) using an accelerating voltage of the electron beam of 200 kV. The samples were prepared by NP dispersions (1 mg mL^{-1} in water) onto a 3 mm copper grid (lacey, 400 mesh) and letting them dry under air at room temperature. The obtained microscopy images were analyzed with the software ImageJ. To determine the elemental composition of the NPs, energy dispersive X-ray spectroscopy with two silicon drift detectors was used during TEM analysis. The counting time for the X-ray spectra was 60 s.

Silicon Metasurface Fabrication: The silicon metasurface with a 5 cm × 5 cm area was designed and produced by the soft-nanoimprinting lithography method.[28,36] A nanopillar array with a hexagonal lattice constant (p) of 1000 nm, a nanopillar diameter d = 400 nm and height h = 500 nm containing silicon substrate (Eulitha) was used as a master structure. A polydimethylsiloxane (PDMS) stamp was prepared by molding on the silicon master structure. The fabrication proceeded by spin coating of a glass substrate with UV/thermally curable sol–gel for imprinting and followed by attachment of the PDMS stamp on the sol–gel. The sol–gel was transformed into substoichiometric silicon dioxide (SiO_x) after UV curing for 5 min.[36] After detaching the PDMS stamp from the substrate, a post-thermal-annealing at 100 °C for 8 min was applied so that residual solvent on the substrate was removed. The NIL process was completed by a second annealing procedure at 600 °C for 1 h to test the thermal stability of the SiO_x nanostructures before further processing. As a final product, a SiO_x replica of the master structure was obtained on the glass substrate. For details on the fabrication of the SiO_x nanopillar array on glass, please also see Figure S1 in the Supporting Information.

Silicon was preferred as dielectric material owing to its optical transparency on NIR-II optical window and high dielectric contrast to nanoparticle/air and glass interface.[36] An 80 nm thick amorphous Si layer was deposited on the SiO_x nanopillars by electron-beam-assisted physical vapor deposition method at 300 °C. The deposited amorphous silicon layer was crystallized at 600 °C under a nitrogen atmosphere. However, the silicon layer around the SiO_x pillars did not crystallize effectively. An electronic grade polysilicon etchant consisting of nitric, phosphoric, and hydrofluoric acid was applied to remove the amorphous silicon layer around the SiO_x nanopillars so that SiO_x nanopillars became vulnerable to breaking under applied gentle mechanical force. After the sample was exposed to polysilicon etchant, trenches formed around SiO_x nanopillars. Next, the SiO_x nanopillars were removed completely from the bottom of the trenches by mechanical abrasion. After the etching process, the silicon layer thickness (t) was reduced to more than 30% of its initial value. As a final product, a nanohole array silicon metasurface with p = 1000 nm, d = 400 nm, and silicon layer thickness t = 53 nm was produced and schematically illustrated in Figure 2a. A scanning electron microscope 30° tilted cross-section image of the produced silicon metasurface is shown in Figure 2b. For details regarding the silicon metasurface production on nanoimprinted glass, please also see Figure S2 in the Supporting Information.

$NaYF_4$:Er^{3+} Nanoparticle Deposition: The produced β-$NaYF_4$:Er^{3+} NPs in cyclohexane solution were deposited on the silicon metasurface and the planar silicon reference via drop-casting. A cross-section of the 660 nm thick β-$NaYF_4$:Er^{3+} nanoparticle layer on metasurface is shown in Figure 2d. A top view is shown in Figure 2c. All the production procedure except nanostructuring was applied simultaneously on a planar silicon reference sample.

Optical Simulations Using the Finite-Element Method: In order to understand the mechanism of the enhanced upconversion luminescence, optical simulations were performed using a commercial finite element solver.[37] The hexagonal unit cell of the periodic metasurface with nanoparticle coating was meshed in 3D using periodic boundaries in the x–y-plane and perfectly matched layer boundaries in the z-direction. A plane wave excitation was used for all simulations. The reflectance and transmittance were calculated by taking the Fourier transform of the outgoing wave solution and summing the power fluxes in the z-direction. The local field enhancement was determined by integrating the electric field energy density over the volume of the nanoparticle coating. In order to account for the line width of the laser source, the local field enhancement was calculated for wavelengths corresponding to the laser line shape, then subsequently multiplied with a Gaussian fit to the laser line shape and integrated over the corresponding wavelength range.

A maximum mesh length of half the material-dependent wavelength was used in combination with adaptive finite element degree (p) elements with a target precision of 1%. Values of p between 2 and

4 were typically employed. Convergence tests confirmed that the desired precision was reached.

A fixed refractive index of 1 was assumed for the air superspace. The refractive index data for the glass substrate and silicon metasurface were taken from literature.[38,39] To obtain the refractive index of the porous nanoparticle film, a Bruggeman effective medium was employed using literature data for the nanoparticles with weight fraction 0.6 and air with weight fraction 0.4.[40,41]

Supporting Information

Supporting Information is available from the Wiley Online Library or from the author.

Acknowledgements

P.M. thanks the Helmholtz Association for funding within the Helmholtz Excellence Network SOLARMATH, a strategic collaboration of Helmholtz-Zentrum Berlin and the DFG center of excellence MATH+ (Grant No. ExNet-0042-Phase-2-3). The optical simulations were done at the Berlin Joint Lab for Optical Simulations for Energy Research (BerOSE). The authors gratefully acknowledge financial support from the DFG (Grant No. SCHA 1009/17-1).

Open access funding enabled and organized by Projekt DEAL.

Conflict of Interest

The authors declare no conflict of interest.

Data Availability Statement

The data that support the findings of this study are available from the corresponding author upon reasonable request.

Keywords

emission enhancement, metasurfaces, nanoparticles, telecommunication wavelengths, third biological excitation window, upconversion

Received: June 24, 2021
Revised: August 28, 2021
Published online: October 6, 2021

[1] A. Shalav, B. S. Richards, T. Trupke, K. W. Krämer, H. U. Güdel, *Appl. Phys. Lett.* **2005**, *86*, 013505.
[2] S. Fischer, J. C. Goldschmidt, P. Löper, G. H. Bauer, R. Brüggemann, K. Krämer, D. Biner, M. Hermle, S. W. Glunz, *J. Appl. Phys.* **2010**, *108*, 044912.
[3] L. Wang, Y. Li, *Chem. Commun.* **2006**, 2557.
[4] Q. Liu, Y. Sun, T. Yang, W. Feng, C. Li, F. Li, *J. Am. Chem. Soc.* **2011**, *133*, 17122.
[5] Z. Qiu, J. Shu, D. Tang, *Anal. Chem.* **2018**, *90*, 12214.
[6] R. G. Geitenbeek, P. T. Prins, W. Albrecht, A. van Blaaderen, B. M. Weckhuysen, A. Meijerink, *J. Phys. Chem. C* **2017**, *121*, 3503.
[7] C. Würth, P. Manley, R. Voigt, D. Ahiboz, C. Becker, U. Resch-Genger, *Nano Lett.* **2020**, *20*, 6682.
[8] W. T. Carnall, P. R. Fields, K. Rajnak, *J. Chem. Phys.* **1968**, *49*, 4424.
[9] D. Saleta Reig, B. Grauel, V. A. Konyushkin, A. N. Nakladov, P. P. Fedorov, D. Busko, I. A. Howard, B. S. Richards, U. Resch-Genger, S. V. Kuznetsov, A. Turshatov, C. Würth, *J. Mater. Chem. C* **2020**, *8*, 4093.
[10] S. Fischer, B. Fröhlich, H. Steinkemper, K. W. Krämer, J. C. Goldschmidt, *Sol. Energy Mater. Sol. Cells* **2014**, *122*, 197.
[11] E. Hemmer, A. Benayas, F. Légaré, F. Vetrone, *Nanoscale Horiz.* **2016**, *1*, 168.
[12] H. Xu, Z. Zhu, J. Xue, Q. Zhan, Z. Zhou, X. Wang, *Photonics Res.* **2021**, *9*, 395.
[13] H. Wang, Z. Yin, W. Xu, D. Zhou, S. Cui, X. Chen, H. Cui, H. Song, *Nanoscale* **2016**, *8*, 10004.
[14] C. Gong, W. Liu, N. He, H. Dong, Y. Jin, S. He, *Nanoscale* **2019**, *11*, 1856.
[15] C. Mao, K. Min, K. Bae, S. Cho, T. Xu, H. Jeon, W. Park, *ACS Photonics* **2019**, *6*, 1882.
[16] L. Liang, D. B. L. Teh, N.-D. Dinh, W. Chen, Q. Chen, Y. Wu, S. Chowdhury, A. Yamanaka, T. C. Sum, C.-H. Chen, N. V. Thakor, A. H. All, X. Liu, *Nat. Commun.* **2019**, *10*, 1391.
[17] G. E. Arnaoutakis, J. Marques-Hueso, A. Ivaturi, S. Fischer, J. C. Goldschmidt, K. W. Krämer, B. S. Richards, *Sol. Energy Mater. Sol. Cells* **2015**, *140*, 217.
[18] J. Christiansen, J. Vester-Petersen, S. Roesgaard, S. H. Møller, R. E. Christiansen, O. Sigmund, S. P. Madsen, P. Balling, B. Julsgaard, *Sol. Energy Mater. Sol. Cells* **2020**, *208*, 110406.
[19] H. Lakhotiya, S. P. Madsen, S. Roesgaard, J. Vester-Petersen, B. B. Iversen, P. Balling, B. Julsgaard, *J. Phys. Chem. C* **2020**, *124*, 22357.
[20] P. Manley, M. Segantini, D. Ahiboz, M. Hammerschmidt, G. Arnaoutakis, R. W. MacQueen, S. Burger, C. Becker, *APL Photonics* **2021**, *6*, 036103.
[21] A. I. Kuznetsov, A. E. Miroshnichenko, M. L. Brongersma, Y. S. Kivshar, B. Luk'yanchuk, *Science* **2016**, *354*, aag2472.
[22] A. Tittl, A. Leitis, M. Liu, F. Yesilkoy, D.-Y. Choi, D. N. Neshev, Y. S. Kivshar, H. Altug, *Science* **2018**, *360*, 1105.
[23] S. Wilhelm, M. Kaiser, C. Würth, J. Heiland, C. Carrillo-Carrion, V. Muhr, O. S. Wolfbeis, W. J. Parak, U. Resch-Genger, T. Hirsch, *Nanoscale* **2015**, *7*, 1403.
[24] B. S. Richards, A. Shalav, *IEEE Trans. Electron Devices* **2007**, *54*, 2679.
[25] W. Wei, Y. Zhang, R. Chen, J. Goggi, N. Ren, L. Huang, K. K. Bhakoo, H. Sun, T. T. Yang Tan, *Chem. Mater.* **2014**, *26*, 5183.
[26] C. Lee, H. Park, W. Kim, S. Park, *Phys. Chem. Chem. Phys.* **2019**, *21*, 24026.
[27] A. Baride, P. S. May, M. T. Berry, *J. Phys. Chem. C* **2020**, *124*, 2193.
[28] D. Ahiboz, P. Manley, C. Becker, *OSA Continuum* **2020**, *3*, 971.
[29] N. Ganesh, W. Zhang, P. C. Mathias, E. Chow, J. A. N. T. Soares, V. Malyarchuk, A. D. Smith, B. T. Cunningham, *Nat. Nanotechnol.* **2007**, *2*, 515.
[30] V. N. Astratov, D. M. Whittaker, I. S. Culshaw, R. M. Stevenson, M. S. Skolnick, T. F. Krauss, R. M. De La Rue, *Phys. Rev. B* **1999**, *60*, R16255.
[31] W. Niu, L. T. Su, R. Chen, H. Chen, Y. Wang, A. Palaniappan, H. Sun, A. I. Yoong Tok, *Nanoscale* **2014**, *6*, 817.
[32] M. Pollnau, D. R. Gamelin, S. R. Lüthi, H. U. Güdel, M. P. Hehlen, *Phys. Rev. B* **2000**, *61*, 3337.
[33] G. N. van den Hoven, E. Snoeks, A. Polman, C. van Dam, J. W. M. van Uffelen, M. K. Smit, *J. Appl. Phys.* **1996**, *79*, 1258.
[34] K.-Y. Pham, L.-C. Wang, C.-C. Hsieh, Y.-P. Hsu, L.-C. Chang, W.-P. Su, Y.-H. Chien, C.-S. Yeh, *J. Mater. Chem. B* **2021**, *9*, 694.
[35] D. Avram, I. Tiseanu, B. S. Vasile, M. Florea, C. Tiseanu, *Sci. Rep.* **2018**, *8*, 18033.

[36] C. Becker, P. Wyss, D. Eisenhauer, J. Probst, V. Preidel, M. Hammerschmidt, S. Burger, *Sci. Rep.* **2015**, *4*, 5886.
[37] J. Pomplun, S. Burger, L. Zschiedrich, F. Schmidt, *Phys. Status Solidi B* **2007**, *244*, 3419.
[38] B. I. Johnson, C. V. Cushman, J. Rowley, B. M. Lunt, N. J. Smith, A. Martin, M. R. Linford, *Surf. Sci. Spectra* **2017**, *24*, 026002.
[39] E. D. Palik, *Handbook of Optical Constants of Solids*, Vol. *3*, Academic Press, **1998**.
[40] V. I. Sokolov, A. V. Zvyagin, S. M. Igumnov, S. I. Molchanova, M. M. Nazarov, A. V. Nechaev, A. G. Savelyev, A. A. Tyutyunov, E. V. Khaydukov, V. Y. Panchenko, *Opt. Spectrosc.* **2015**, *118*, 609.
[41] D. A. G. Bruggeman, *Ann. Phys. (Leipzig)* **1935**, *416*, 636.